analytical chemistry

pubs.acs.org/ac Article

Molecular Perturbation Effects in AFM-Based Tip-Enhanced Raman Spectroscopy: Contact versus Tapping Mode

Giovanni Luca Bartolomeo, Yao Zhang, Naresh Kumar,* and Renato Zenobi*

Cite This: *Anal. Chem.* 2021, 93, 15358−15364 Read Online

ACCESS | Metrics & More | Article Recommendations | Supporting Information

ABSTRACT: Tip-enhanced Raman spectroscopy (TERS) is a powerful tool for nondestructive and label-free surface chemical characterization at nanometer length scales. However, despite being considered nondestructive, the interaction of the TERS probe used in the analysis can alter the molecular organization of the sample. In this study, we investigate the role of the atomic force microscopy (AFM) feedback (contact mode and tapping mode) on molecular perturbation in TERS analysis of soft samples using a self-assembled monolayer (SAM) of 2-chloro-4-nitrobenzene-1-thiol (Cl-NBT) as a test sample. Surprisingly, the tapping mode shows a consistently higher TERS signal resulting from a minimal perturbation of the Cl-NBT SAM compared to the contact mode. This study provides novel insights into the choice of the correct AFM-TERS operation mode for nanoscale chemical analysis of soft and delicate samples and is expected to expedite the growing application of TERS in this area.

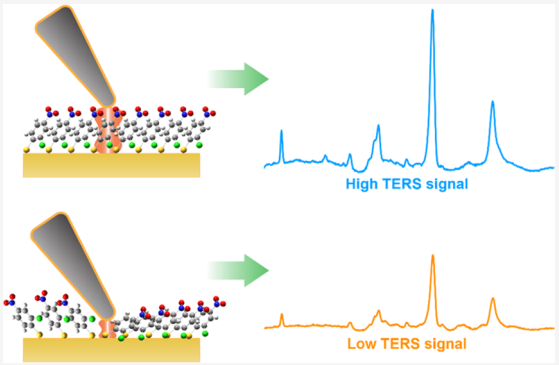

INTRODUCTION

The interest of the scientific community in nanotechnologies has increased substantially in the last few decades, leading to the development of powerful tools to characterize nanostructured materials with higher sensitivity and spatial resolution than ever before. Today, several nano-analytical techniques are available, each having its own strengths and limitations. However, nondestructive and label-free nanoscale molecular imaging under ambient conditions still remains challenging. For example, nanoscale secondary ion mass spectrometry (nanoSIMS) can provide elemental and isotopic information with a spatial resolution of down to tens of nanometers but requires the sample to be compatible with ultrahigh vacuum conditions and easily ionizable, and is destructive.[1,2] On the other hand, super-resolution fluorescence microscopy provides a spatial resolution down to *ca.* 25 nm nondestructively but requires fluorophore labeling that can alter the native state of the sample.[3,4] When noninvasiveness is the highest priority, especially for the study of delicate systems in their native state, label-free spectroscopies, such as nanoscale infrared (nanoIR) spectroscopy and tip-enhanced Raman spectroscopy (TERS), are the techniques of choice. Nano-IR combines scanning probe microscopy (SPM) with IR spectroscopy and provides nondestructive chemical and topographical information.[5] However, single-molecule resolution is not possible and application in liquid environments is limited.[6]

TERS overcomes most of these limitations and provides nondestructive and label-free molecular imaging at the nanoscale level in both air and liquid environments.[7,8] In TERS, a metallic SPM tip is used to dramatically enhance the electromagnetic (EM) field in the focal spot of an excitation laser and confine the EM field within a nanoscopic volume *via* a combination of localized surface plasmon resonance and lightning rod effect.[9] The spatially confined optical field enhancement in TERS can provide single-molecule sensitivity with angstrom-scale resolution.[10] TERS can be performed in both atomic force microscopy (AFM) and scanning tunneling microscopy (STM) SPM modes.[11] However, since AFM feedback does not necessitate an electrical contact with the sample, AFM-TERS is more versatile allowing a much wider range of applications including organic solar cells,[12] biological cells,[13] DNA strands,[14] lipid membranes, two-dimensional (2D) nanomaterials,[15,16] and catalytic materials.[17−19] AFM-TERS is most commonly operated using either the contact or tapping mode feedback. In contact mode,[7] the AFM probe simply scans the sample and the resulting cantilever deflection is measured; whereas in tapping mode,[20,21] which is a milder interaction regime, the sample is imaged by measuring the reduction in amplitude of an oscillating probe put in close proximity to a surface.[22] Although both contact and tapping modes have been successfully used to perform TERS

Received: July 17, 2021
Accepted: October 25, 2021
Published: November 12, 2021

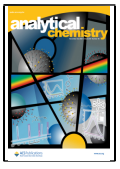

https://doi.org/10.1021/acs.analchem.1c03004
Anal. Chem. 2021, 93, 15358−15364

measurements,[14,16,23] to the best of our knowledge, the influence of the AFM feedback mode on molecular perturbation in chemical analysis using TERS has never been investigated.

In this work, we perform a comparative study of TERS measurements using contact and tapping mode AFM. Both AFM modes are applied on a self-assembled monolayer (SAM) of 2-chloro-4-nitrobenzene-1-thiol (Cl-NBT) using TERS probes with a similar Au coating. Intuitively, we expected a higher TERS signal in contact mode AFM-TERS because of the closer proximity of the probe to the sample. Nevertheless, interestingly, a consistently higher TERS signal is observed in tapping mode compared to contact mode. After a detailed analysis of Cl-NBT vibrational modes supported by density functional theory (DFT) calculations, we attribute the higher TERS signal in tapping mode to the lower molecular perturbation of the Cl-NBT SAM. Our results highlight a subtle but important role of the AFM feedback in choosing the correct operational mode for chemical analysis of soft and delicate molecular samples using TERS.

EXPERIMENTAL SECTION

TERS System. TERS experiments were performed on an NTEGRA Spectra II TERS system (NT-MDT Spectrum Instruments, Russia) equipped with an AFM and a Raman spectrometer in top illumination geometry. A schematic representation of the setup is depicted in Figure 1. A 632.8 nm He−Ne laser (LASOS, Germany) was focused onto the sample using a 100×, 0.9 NA objective (Olympus, Japan). Unless otherwise specified, a laser power of 10 μW was utilized on the sample surface for TERS measurements with a spectrum acquisition time of 2 s. In contact mode, a vertical force of ∼9 nN was applied to the sample (see Table S1 for details). In tapping mode, a free oscillation amplitude of ∼100 nm was imposed and the oscillation amplitude of the probe in contact with the sample was set to 70% of the free oscillation. After bringing the probe in contact with the sample, the oscillation amplitude was rechecked through amplitude−distance curves. In tapping mode, a maximum vertical force of ∼1570 nN was applied to the sample (see Table S2 for details). Note that although the maximum vertical force in the tapping mode is nearly 2 orders of magnitude higher than the contact mode, the lateral force is expected to be significantly higher in contact mode,[24] potentially resulting in a substantial disruption of analyte molecules.

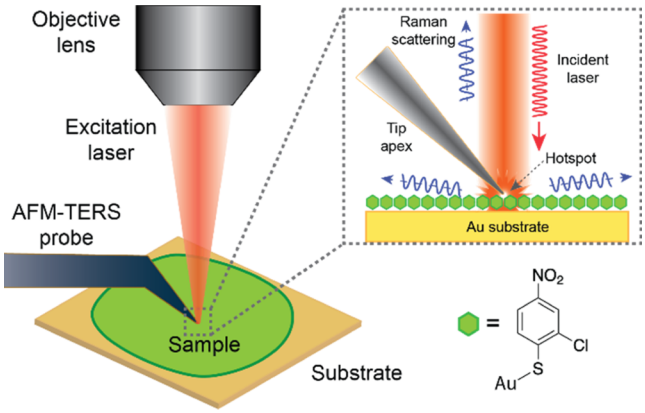

Figure 1. Schematic representation of the TERS setup used to study molecular perturbation effects in chemical analysis using TERS.

TERS Probes. ATEC-NC and ATEC-CONT Si AFM cantilevers (NanoAndMore, Germany) were used to prepare contact mode and tapping mode TERS probes. To increase the refractive index of the surface,[25] Si cantilevers were oxidized in a furnace (Carbolite Gero, U.K.) at 1000 °C for 22.5 h to obtain a SiO_2 layer of ∼300 nm. Before metal coating, oxidized cantilevers were cleaned inside a UV−ozone cleaner (Ossila, United Kingdom) for 1 h. Probes were then coated with Au (99.99%, Acros Organics) to a nominal thickness of 100 nm at 0.02 nm/s and a pressure of $<10^{-6}$ mbar inside a thermal evaporation system (MBraun, Germany). To prepare contamination-free TERS probes with high plasmonic sensitivity, the entire thermal evaporation system was placed inside a nitrogen glovebox (MBraun, Germany) with <0.1 ppm of oxygen and moisture.

Preparation of Cl-NBT SAM on Au. Ultraflat Au substrates were prepared using the template-stripping method.[26] Cl-NBT SAM was constructed by soaking the Au substrates within a 5 mM solution of Cl-NBT in ethanol for 12 h. Cl-NBT SAM samples were rinsed with a copious amount of ethanol and dried under nitrogen before use.

Scanning Electron Microscopy (SEM). SEM imaging was performed using a Hitachi SU5000 instrument (Hitachi, Japan) with an acceleration voltage of 5 kV and a current intensity of 0.1 nA. SEM imaging of the probes was carried out after TERS measurements.

Density Functional Theory (DFT) Calculations. Raman vibrational modes of Cl-NBT were simulated with Gaussian 9.0 and GaussView 5.0 softwares (Gaussian Inc.) using B3LYP hybrid functional and the 6-31G(+) basis set. Orientation-dependent DFT simulations of the Raman spectra of Cl-NBT and Cl-NBT-Au were performed using in-house-developed scripts in MATLAB R2021a.

Data Analysis. AFM and SEM images were processed using Gwyddion software (gwyddion.net). Spectral data were analyzed and plotted using a custom-made Python routine. TERS spectra were background-subtracted using an asymmetric-least-squared algorithm prior to Gaussian fitting of peaks as illustrated in Figure S1. TERS signal intensity was evaluated from the fitted peak height.

RESULTS AND DISCUSSION

The Cl-NBT SAM used in this study produces a strong TERS signal[27] however, it is also deformable[28] making it a good model system for the investigation of the probe-sample interaction. An AFM topography image of the Cl-NBT SAM is shown in Figure 2a, which shows a smooth topography with RMS roughness of 0.6 nm. To rule out the possibility of any surface-enhanced Raman spectroscopy (SERS) contribution from the Au substrate, far-field Raman imaging of the sample was first performed. However, no Raman bands were observed as shown in the far-field spectrum in Figure S2, confirming the SERS inactivity of the Au substrate. The Au coating of the probes was examined using SEM, as shown in Figures 2b,c, S3, and S4 (top panels). All TERS probes showed a similarly homogeneous Au coating. Moreover, the contact mode and tapping mode TERS probes exhibited a similar apex diameter as listed in Table S3.

To compare TERS signals in contact and tapping modes, we carried out TERS imaging of the Cl-NBT SAM on Au in each mode with five different probes in 2 μm × 2 μm areas with 20

https://doi.org/10.1021/acs.analchem.1c03004
Anal. Chem. 2021, 93, 15358−15364

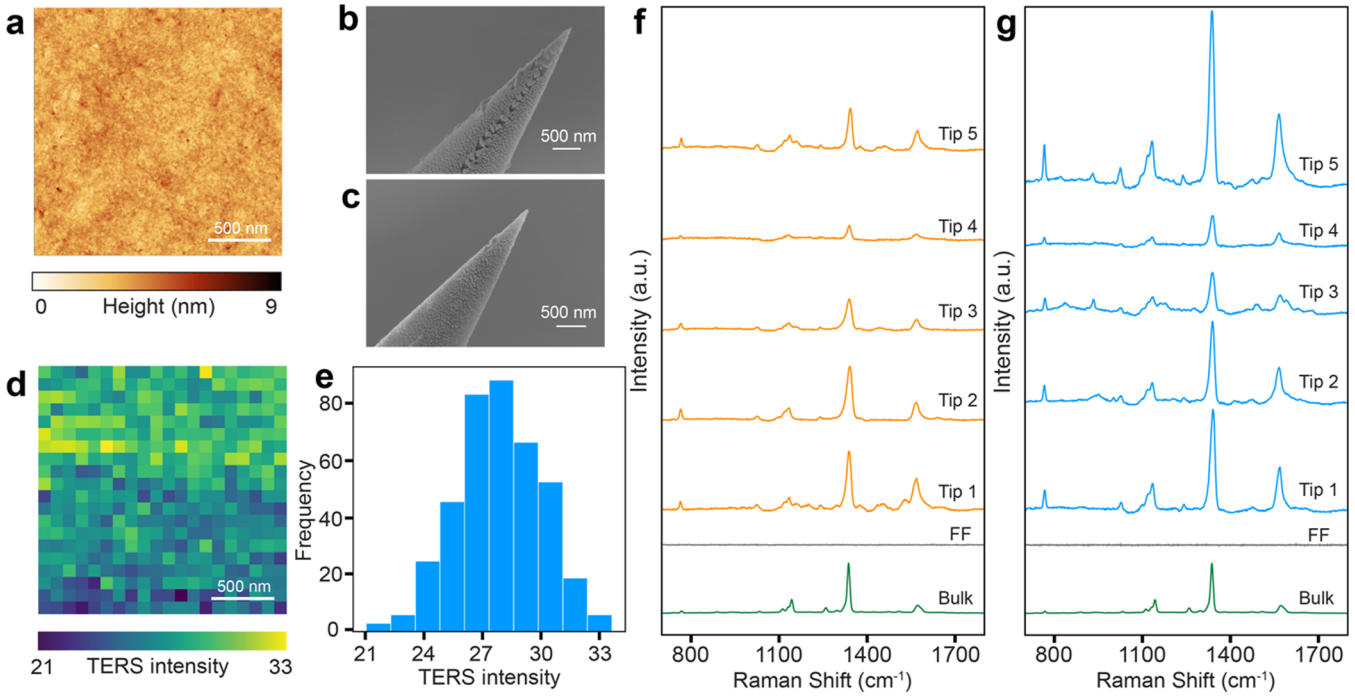

Figure 2. (a) AFM topography image of the Cl-NBT SAM on a Au substrate. SEM images of representative Au-coated (b) contact mode and (c) tapping mode TERS probes. (d) TERS image (20 × 20 pixels) of the 1336 cm^{-1} signal intensity measured using tapping mode AFM feedback. (e) Histogram of signal intensity in the TERS image shown in (d). Averaged spectra of the TERS images of the Cl-NBT SAM on Au measured using five different probes in (f) contact mode and five different probes in (g) tapping mode. Each spectrum represents an average of 400 spectra measured within a TERS image. Far-field (FF) confocal Raman spectra measured with the TERS probes retracted from the sample and confocal Raman spectrum of bulk Cl-NBT are also plotted for comparison. Both (f) and (g) share the same *y*-axis; the spectra are vertically shifted for easier visualization.

× 20 pixels (400 spectra). A representative TERS image of the 1336 cm^{-1} signal ($-NO_2$ stretching mode) intensity measured in the tapping mode is shown in Figure 2d. Rather consistent TERS spectra of the sample were recorded throughout the image, demonstrating the stability of the TERS system. Nonetheless, a spatial variation in the signal intensity is observed across the TERS image, possibly coming from the variation in the plasmonic resonance of the Au-coated tip-Au substrate geometry. A similar behavior is observed in the TERS images measured with other tapping mode and contact mode probes as shown in Figures S3 and S4 (middle panels), respectively. Note that spurious signals, possibly from organic contaminants, were also observed in some spectra in the TERS images measured using both tapping and contact modes, as shown in Figure S5. However, since such spurious signals are observed randomly, their contribution to the average spectrum is minimal. A histogram of the TERS signal intensity measured in Figure 2d is shown in Figure 2e, which shows only a small intensity variation indicating good probe stability and consistency of the tip-substrate plasmon resonance. Intensity histograms of other TERS images measured in tapping and contact modes are shown in Figures S3 and S4 (bottom panels).

Average spectra of the TERS images measured in tapping and contact modes are plotted in Figure 2f,g, respectively, together with the far-field Raman spectra of Cl-NBT SAM and Raman spectrum of bulk Cl-NBT. All TERS spectra show a very good correlation of the band positions with the Raman spectrum of bulk Cl-NBT. A summary of the TERS results is shown in Figure 3. Figure 3a shows a comparison of the average intensity of the 1336 cm^{-1} signal measured in TERS images (400 spectra in total) using five different probes in tapping and contact modes, respectively. Small error bars in the TERS signal of most probes indicate the stability of plasmonic signal enhancement of the Cl-NBT SAM on Au. Interestingly, in tapping mode, a higher TERS signal is consistently observed for all five probes compared to the contact mode. This trend is even more clear in Figure 3b, where in the comparison of average TERS spectra measured in all TERS images (2000 spectra), TERS signal in tapping mode is found to be 2.5 times higher than contact mode. Despite the difference in signal intensity, the average TERS spectra measured in contact and tapping modes showed no significant difference from the far-field Raman spectrum in terms of peak positions and relative peak intensity, as shown in Figure S6.

In TERS geometry of a metallic tip in contact with a metal substrate, also known as "gap mode", the plasmonically enhanced optical field is confined to a nanoscopic volume. It has been well established from a number of experimental and theoretical TERS studies that the gap-mode, TERS enhancement decreases dramatically over a distance of *ca.* 3 nm[29] and becomes negligible above 5 nm,[30] as summarized in Table S4. Tapping mode TERS probes typically oscillate with a frequency of 210 490 kHz spending only a fraction of time in contact with the Cl-NBT SAM in contrast to contact mode, in which TERS probes remain virtually stationary and in contact with the sample at all times.[31] Therefore, the observation of a higher TERS signal in tapping mode shown in Figure 3a,b is counterintuitive and surprising. In our TERS experiments, tapping mode probes typically oscillate with an amplitude of ~70 nm. Assuming a harmonic oscillator model, the time spent by tapping mode probes in close contact (i.e.,

https://doi.org/10.1021/acs.analchem.1c03004
Anal. Chem. 2021, 93, 15358−15364

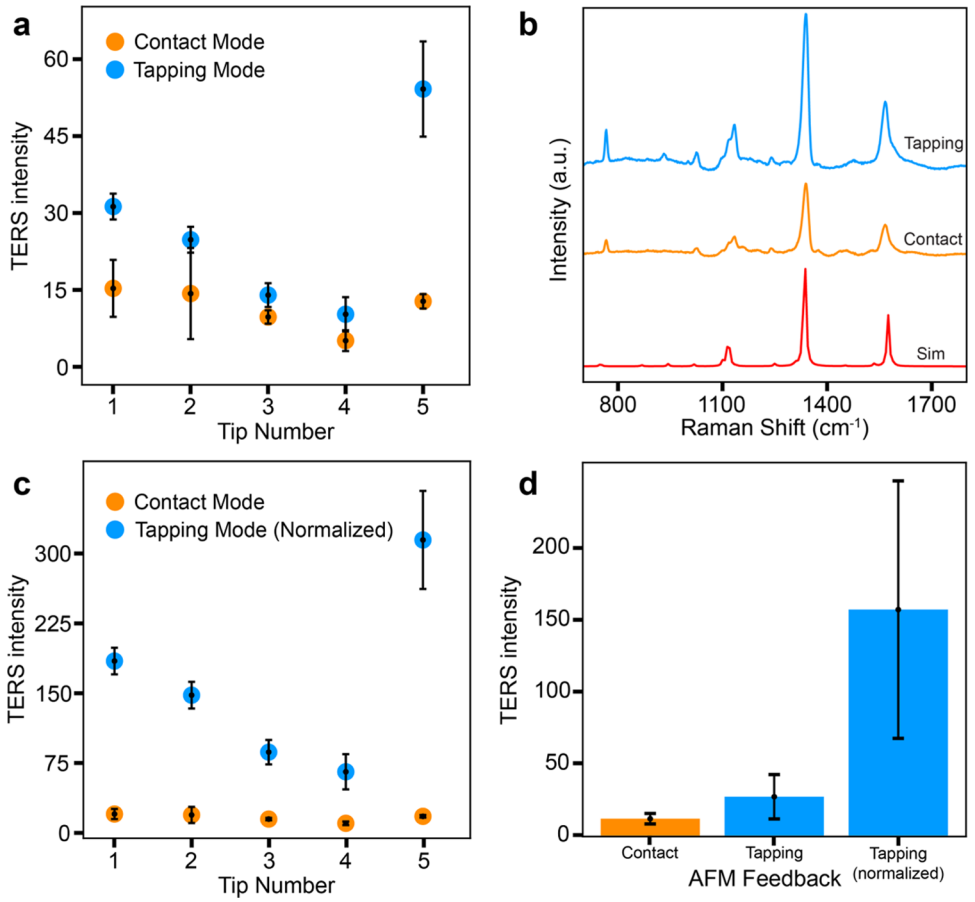

Figure 3. (a) Comparison of average TERS signal intensity measured with contact and tapping mode feedback. Each TERS intensity value represents an average intensity of the 1336 cm^{-1} signal in 400 spectra measured in a TERS image. Error bars represent the standard deviation of the signal over the TERS image. (b) Plot showing an average of 2000 TERS spectra measured using five different TERS probes in contact and tapping modes, respectively. A simulated Raman spectrum of Cl-NBT is also plotted for comparison. (c) Same as plot (a), with the values for tapping mode TERS measurements normalized for the time the TERS probe spends in close proximity to the sample, as discussed in Figure S7. (d) Comparison of the average TERS signal in 2000 TERS spectra measured using contact and tapping modes. Error bars represent the standard deviation of the signal in all TERS spectra measured with a particular feedback mode. "Tapping (normalized)" represents the contact-time-normalized TERS signal in tapping mode.

within less than 5 nm) with the sample is ~17.2% of the total oscillation period, as illustrated in Figure S7. This implies that for the same spectrum integration time, the actual time contributing to the near-field signal in tapping mode is ~6 times shorter compared to contact mode. Normalizing the tapping mode TERS signal intensity with this factor reveals an even higher signal compared to the contact mode as shown in Figure 3c. A comparison of the average signal in 2000 TERS spectra measured in tapping and contact modes is shown in Figure 3d, where the contact-time-normalized TERS signal intensity in tapping mode is found to be 13 times higher than contact mode.

This result is confounding since for the same integration time a higher TERS signal is expected in contact mode as the continuous contact of the probe with the sample will allow a greater sampling of plasmonically enhanced signal. However, contrary to this expectation, a significantly higher TERS signal is observed in tapping mode under identical measurement conditions as shown in Figure 3. To understand this, we need to consider the probe-sample interaction in contact and tapping mode AFM-TERS. Despite careful control of the measurement parameters, soft samples have been shown to alter during AFM imaging in contact mode.[28] We tested this hypothesis in our own setup by performing the AFM imaging of a 1,2-dioleoyl-sn-glycero-3-phosphocholine (DOPC) bilayer lipid grating sample in contact and tapping modes, which is shown in Figure S8. A severe disruption of the surface features is observed in the contact mode (Figure S8a), whereas the lipid grating remains intact in the tapping mode AFM image (Figure S8b) indicating a minimal perturbation of molecular arrangement. On the other hand, the same phenomenon is not observed during the imaging of a silicon grating in contact and tapping modes, which is a relatively hard sample as shown in Figure S8c,d.

The AFM imaging results of a lipid grating may not be directly comparable to a thiol SAM; however, perturbation of the molecular arrangement of thiol molecules in the contact mode AFM imaging cannot be ruled out. In fact, the thiol SAM does not necessarily have to be permanently removed or modified to produce a relatively lower TERS signal. Our group has previously shown that molecular orientation can have significant influence on the intensity of bands in a TERS spectrum.[32] To confirm this, we performed DFT simulation of the Cl-NBT Raman spectrum, which is shown in Figures 3b and S9. The simulated Raman spectrum corroborates the measured TERS spectra very well both in terms of the peak

https://doi.org/10.1021/acs.analchem.1c03004
Anal. Chem. 2021, 93, 15358−15364

position and relative peak intensity. The assignment of the TERS and simulated Raman bands is listed in Table 1. Analysis

Table 1. Assignment of the Main Bands in the TERS and Simulated Raman Spectra of Cl-NBT; See Figure S9 for Further Details

TERS signal (cm^{-1})	simulated signal (cm^{-1})	assignment
1118	1100	C−N stretching
1135	1116	ring breathing
1242	1249	C−H rocking
1336	1336	$-NO_2$ stretching
1567	1574	C=C stretching

of the simulated vibrational modes reveals that all major bands of the spectrum, i.e., ring-breathing mode at 1135 cm^{-1}, $-NO_2$ stretching mode at 1336 cm^{-1}, and C=C stretching mode at 1567 cm^{-1}, represent in-plane modes as shown in Figure 4a−c

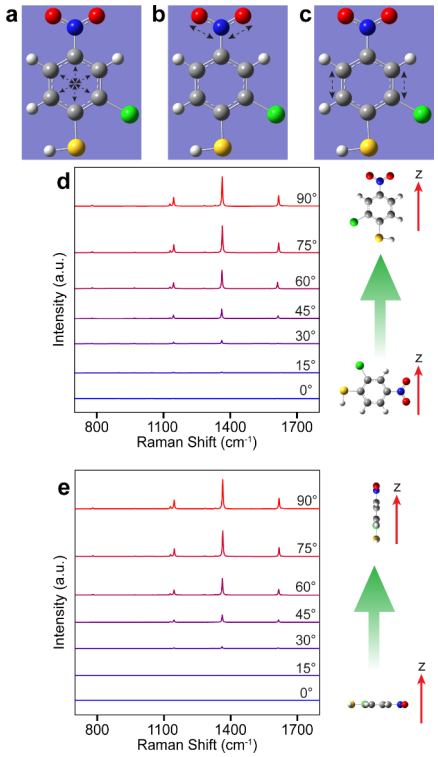

Figure 4. Representation of the in-plane (a) ring-breathing mode at 1135 cm^{-1}, (b) $-NO_2$ stretching mode at 1336 cm^{-1}, and (c) in-plane C=C stretching mode at 1567 cm^{-1} calculated with DFT simulations. DFT simulations of Cl-NBT Raman spectra at different orientation angles with respect to the substrate surface, for molecules lying (d) sideways or (e) flat at 0°. The polarization of incident light is aligned with *z*-axis, which is indicated by a red arrow. In both cases, the intensity of all Raman bands decreases rapidly as the molecule bends toward the substrate surface.

and the Supporting MP4 Files. In a gap-mode TERS configuration, since the plasmonically enhanced optical field has a vertical polarization, these in-plane Raman modes will experience a strong enhancement when the plane of vibration is vertically aligned.[33,34] We tested this hypothesis with DFT calculation of the orientation-dependent Raman spectra of Cl-NBT molecules under irradiation of vertically polarized light. These results are presented in Figure 4d,e, which clearly show a rapid decrease in the intensities of all major Raman bands as the molecule bends toward the substrate surface. Furthermore, the result did not change even when the thiol molecule was bound to a Au atom, as shown in Figure S10.

The experimental and theoretical results strongly indicate that in the tapping mode TERS imaging, the Cl-NBT SAM remains largely unperturbed in which the molecules lie at an angle of 60−70°[35] and a large component of the polarizability tensor of in-plane vibrational modes stands parallel to the vertical polarization of the near-field as schematically illustrated in Figure 5a. However, in contact mode TERS imaging of the Cl-NBT SAM, direct continuous contact of the probe with the sample likely perturbs the molecular arrangement by flattening the molecules, thereby reducing the vertical component of their polarizability tensor as well as the number of molecules in the near-field as illustrated in Figure 5b. The TERS intensity of out-of-plane vibrational modes, for example the out-of-plane wagging at 807 cm^{-1} shown in Figure S9 and animated files available in the Supporting Information, should increase when the molecules are bent by large angles or flattened. However, these vibrational modes are not detectable in the experimental spectrum because of a very low cross section as shown by DFT simulations.

The noninvasiveness of the tapping mode TERS measurements observed in our study corroborates similar results obtained by Wang *et al.* on a different molecular system, where intermittent contact mode was found to be relatively more invasive for molecular analysis.[36] However, in our contact mode TERS measurements (Figures 2f and S6), we did not consistently observe any new Raman bands or the Stark-shifting or broadening of the existing Raman bands, which have been previously attributed to molecular charging,[37] chemical transformation[36] or optical rectification effects.[38] Furthermore, in the last decade, a number of experimental and theoretical studies have demonstrated that the nanogap plasmons within a metallic tip-sample junction are governed by quantum mechanical effects including electron tunneling and nonlocal screening.[39] Particularly, when the tip-sample nanogap becomes ≤1 nm, electron tunneling could lead to a decrease in the intensity of EM field enhancement.[40−42] For example, Zhu *et al.* observed quenching of SERS enhancements of thiophenol molecules adsorbed on Au nanoparticles below an interparticle gap distance of 0.67 nm due to the electron tunneling effect.[40] In our study, the length of the molecular reporter, Cl-NBT, is ∼0.74 nm. Although precise determination of the tip-sample nanogap distance in contact mode is extremely challenging, we expect it to be between 0.74 and 1 nm in our experiments. Therefore, in contact mode TERS measurements, the possibility of quenching of electromagnetic field enhancement due to electron tunneling cannot be completely ruled out.

We propose that in contact mode TERS imaging, the molecular disruption of the Cl-NBT SAM and the possible electron tunneling effect cause a lower signal compared to the tapping mode. Therefore, for nanoscale chemical analysis of "soft samples" such as SAMs of organic molecules or lipid monolayer/bilayer systems in their native state using TERS, tapping mode should be the method of choice because of a lower degree of molecular perturbation as well as lower quantum-mechanical EM field quenching, and, consequently, higher signal intensity.

https://doi.org/10.1021/acs.analchem.1c03004
Anal. Chem. 2021, 93, 15358−15364

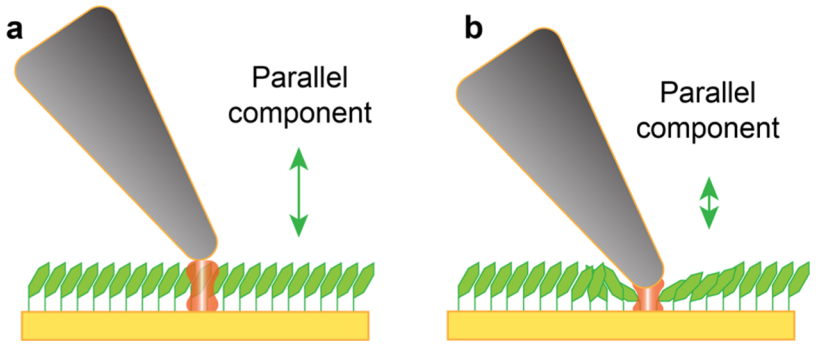

Figure 5. (a) In tapping mode, a minimal molecular disruption results in a higher number of molecules in the near-field as well as a greater plasmonic enhancement of the vertical component of in-plane vibrational modes. (b) In contact mode, the direct contact of the probe with the sample can laterally disrupt the thiol SAM, decreasing the number of molecules inside the near-field as well as changing their orientation.

CONCLUSIONS

In this work, we have performed a comparative study of the influence of AFM feedback on molecular perturbation in chemical analysis using TERS. Despite the conventional belief that "closer is better" in terms of TERS signal enhancement, the data presented herein show that this approach could be counterproductive for soft samples. A consistently higher TERS signal is obtained in tapping mode despite the probe spending 6-fold less time in close proximity to the sample than contact mode. Comparative TERS imaging of soft and hard grating samples indicates that a larger perturbation of the organization and orientation of the probed molecules in contact mode, possibly in combination with electron tunneling induced EM field quenching, diminishes the TERS signal of the probed species. Permanent damage has not been proven but appears to be a likely scenario when working in contact mode, particularly for soft samples that are not chemically bound to the substrate surface. Note that, caution should be exercised in directly applying the results of this study to other "soft" samples as the precise TERS signal difference between contact and tapping modes may be affected by several factors including sample thickness, sample adhesion to the substrate, tip-sample distance, etc. Nevertheless, this study clearly demonstrates that although both tapping and contact modes are capable of producing a TERS signal with a high signal-to-noise ratio, the degree of molecular perturbation could be significantly different. Therefore, for the TERS measurements of soft samples, tapping mode should be the preferred method of choice. The novel insights gained in this study are expected to accelerate the growing application of TERS to non-destructive and label-free nanoscale chemical analysis of delicate samples.

ASSOCIATED CONTENT

Supporting Information

The Supporting Information is available free of charge at https://pubs.acs.org/doi/10.1021/acs.analchem.1c03004.

Supporting figures and tables (Figures S1−S10 and Tables S1−S4) (PDF)

The original data used in this publication are made available in a curated data archive at ETH Zurich (https://www.research-collection.ethz.ch) under the DOI: 10.3929/ethz-b-000487065.

Raman vibrational modes of Cl-NBT (MP4)
Raman vibrational modes of Cl-NBT (MP4)
Raman vibrational modes of Cl-NBT (MP4)
Raman vibrational modes of Cl-NBT (MP4)
Raman vibrational modes of Cl-NBT (MP4)
Raman vibrational modes of Cl-NBT (MP4)
Raman vibrational modes of Cl-NBT (MP4)
Raman vibrational modes of Cl-NBT (MP4)
Raman vibrational modes of Cl-NBT (MP4)
Raman vibrational modes of Cl-NBT (MP4)

AUTHOR INFORMATION

Corresponding Authors

Naresh Kumar − *Department of Chemistry and Applied Biosciences, ETH Zürich, 8093 Zürich, Switzerland;* orcid.org/0000-0001-8953-5420; Email: naresh.kumar@org.chem.ethz.ch

Renato Zenobi − *Department of Chemistry and Applied Biosciences, ETH Zürich, 8093 Zürich, Switzerland;* orcid.org/0000-0001-5211-4358; Email: zenobi@org.chem.ethz.ch

Authors

Giovanni Luca Bartolomeo − *Department of Chemistry and Applied Biosciences, ETH Zürich, 8093 Zürich, Switzerland;* orcid.org/0000-0003-0720-4965

Yao Zhang − *Hefei National Laboratory for Physical Sciences at the Microscale and Synergetic Innovation Center of Quantum Information and Quantum Physics, University of Science and Technology of China, Hefei 230026 Anhui, China; State Key Laboratory of Quantum Optics and Quantum Optics Devices, Shanxi University, Taiyuan 030006, China*

Complete contact information is available at: https://pubs.acs.org/10.1021/acs.analchem.1c03004

Notes

The authors declare no competing financial interest.

ACKNOWLEDGMENTS

The authors thank ScopeM at ETH Zurich for providing access to SEM instrumentation. Christian Marro from ETH mechanical workshop is thanked for technical support. Dr. Guillaume Goubert from ETH Zurich is thanked for helpful discussions. Dr. Liqing Zheng and High-Performance Computing Team at ETH Zurich are thanked for help with DFT calculations. Dr. Eider Berganza Eguiarte and Dr. Michael

Hirtz from Karlsruhe Institute of Technology are thanked for providing lipid grating samples. G.L.B. acknowledges financial support from the Scholarship Fund of Swiss Chemical Industry (SSCI). G.L.B., N.K., and R.Z. acknowledge financial support from the European Union through the ERC Grant No. 741431 2D-NanoSpec. Y.Z. acknowledges financial support from the Program of State Key Laboratory of Quantum Optics and Quantum Optics Devices (Grant No. KF201902).

REFERENCES

(1) Herrmann, A. M.; Ritz, K.; Nunan, N.; Clode, P. L.; Pett-Ridge, J.; Kilburn, M. R.; Murphy, D. V.; O'Donnell, A. G.; Stockdale, E. A. *Soil Biol. Biochem.* **2007**, *39*, 1835−1850.
(2) Kailas, L.; Audinot, J. N.; Migeon, H. N.; Bertrand, P. *Compos. Interfaces* **2006**, *13*, 423−439.
(3) Huang, B.; Bates, M.; Zhuang, X. *Annu. Rev. Biochem.* **2009**, *78*, 993−1016.
(4) Schermelleh, L.; Heintzmann, R.; Leonhardt, H. *J. Cell Biol.* **2010**, *190*, 165−175.
(5) Knoll, B.; Keilmann, F. *Nature* **1999**, *399*, 134−137.
(6) Huth, F.; Govyadinov, A.; Amarie, S.; Nuansing, W.; Keilmann, F.; Hillenbrand, R. *Nano Lett.* **2012**, *12*, 3973−3978.
(7) Kumar, N.; Weckhuysen, B. M.; Wain, A. J.; Pollard, A. J. *Nat. Protoc.* **2019**, *14*, 1169−1193.
(8) Wang, X.; Huang, S.-C.; Hu, S.; Yan, S.; Ren, B. *Nat. Rev. Phys.* **2020**, *2*, 253−271.
(9) Kumar, N.; Mignuzzi, S.; Su, W.; Roy, D. *EPJ Tech. Instrum.* **2015**, *2*, No. 9.
(10) Lee, J.; Crampton, K. T.; Tallarida, N.; Apkarian, V. A. *Nature* **2019**, *568*, 78−82.
(11) Verma, P. *Chem. Rev.* **2017**, *117*, 6447−6466.
(12) Kumar, N.; Zoladek-Lemanczyk, A.; Guilbert, A. A. Y.; Su, W.; Tuladhar, S. M.; Kirchartz, T.; Schroeder, B. C.; McCulloch, I.; Nelson, J.; Roy, D.; Castro, F. A. *Nanoscale* **2017**, *9*, 2723−2731.
(13) Kumar, N.; Drozdz, M. M.; Jiang, H.; Santos, D. M.; Vaux, D. J. *Chem. Commun.* **2017**, *53*, 2451−2454.
(14) He, Z.; Han, Z.; Kizer, M.; Linhardt, R. J.; Wang, X.; Sinyukov, A. M.; Wang, J.; Deckert, V.; Sokolov, A. V.; Hu, J.; Scully, M. O. *J. Am. Chem. Soc.* **2019**, *141*, 753−757.
(15) Legge, E. J.; Paton, K. R.; Wywijas, M.; McMahon, G.; Pemberton, R.; Kumar, N.; Aranga Raju, A. P.; Dawson, C. P.; Strudwick, A. J.; Bradley, J. W.; Stolojan, V.; Silva, S. R. P.; Hodge, S. A.; Brennan, B.; Pollard, A. J. *ACS Appl. Mater. Interfaces* **2020**, *12*, 13481−13493.
(16) Kumar, N.; Marchesini, S.; Howe, T.; Edwards, L.; Brennan, B.; Pollard, A. J. *J. Chem. Phys.* **2020**, *153*, No. 184708.
(17) Lipiec, E.; Sekine, R.; Bielecki, J.; Kwiatek, W. M.; Wood, B. R. *Angew. Chem., Int. Ed.* **2014**, *53*, 169−172.
(18) Nakata, A.; Nomoto, T.; Toyota, T.; Fujinami, M. *Anal. Sci.* **2013**, *29*, 865−869.
(19) Kumar, N.; Kalirai, S.; Wain, A. J.; Weckhuysen, B. M. *ChemCatChem* **2019**, *11*, 417−423.
(20) vandenAkker, C. C.; Deckert-Gaudig, T.; Schleeger, M.; Velikov, K. P.; Deckert, V.; Bonn, M.; Koenderink, G. H. *Small* **2015**, *11*, 4131−4139.
(21) Deckert-Gaudig, T.; Böhme, R.; Freier, E.; Sebesta, A.; Merkendorf, T.; Popp, J.; Gerwert, K.; Deckert, V. *J. Biophotonics* **2012**, *5*, 582−591.
(22) Voigtländer, B. *Scanning Probe Microscopy*; Springer, 2015.
(23) Bartolomeo, G. L.; Goubert, G.; Zenobi, R. *Appl. Spectrosc.* **2020**, *74*, 1358−1364.
(24) Hölscher, H. *Encyclopedia of Nanotechnology*; In Bhushan, B., Ed.; Springer Netherlands: Dordrecht, 2012; p 99.
(25) Yeo, B.-S.; Schmid, T.; Zhang, W.; Zenobi, R. *Anal. Bioanal. Chem.* **2007**, *387*, 2655−2662.
(26) Weiss, E. A.; Kaufman, G. K.; Kriebel, J. K.; Li, Z.; Schalek, R.; Whitesides, G. M. *Langmuir* **2007**, *23*, 9686−9694.
(27) Yin, H.; Zheng, L.-Q.; Fang, W.; Lai, Y.-H.; Porenta, N.; Goubert, G.; Zhang, H.; Su, H.-S.; Ren, B.; Richardson, J. O.; Li, J.-F.; Zenobi, R. *Nat. Catal.* **2020**, *3*, 834−842.
(28) Moores, B.; Simons, J.; Xu, S.; Leonenko, Z. *Nanoscale Res. Lett.* **2011**, *6*, No. 185.
(29) Ichimura, T.; Fujii, S.; Verma, P.; Yano, T.; Inouye, Y.; Kawata, S. *Phys. Rev. Lett.* **2009**, *102*, No. 186101.
(30) Pettinger, B.; Domke, K. F.; Zhang, D.; Picardi, G.; Schuster, R. *Surf. Sci.* **2009**, *603*, 1335−1341.
(31) Slade, A. L.; Yip, C. M. *Molecular Interfacial Phenomena of Polymers and Biopolymers*; In Chen, P., Ed.; Woodhead Publishing, 2005; pp 161−213.
(32) Shao, F.; Müller, V.; Zhang, Y.; Schlüter, A. D.; Zenobi, R. *Angew. Chem., Int. Ed.* **2017**, *56*, 9361−9366.
(33) Jiang, N.; Chiang, N.; Madison, L. R.; Pozzi, E. A.; Wasielewski, M. R.; Seideman, T.; Ratner, M. A.; Hersam, M. C.; Schatz, G. C.; Van Duyne, R. P. *Nano Lett.* **2016**, *16*, 3898−3904.
(34) Jiang, S.; Zhang, Y.; Zhang, R.; Hu, C.; Liao, M.; Luo, Y.; Yang, J.; Dong, Z.; Hou, J. G. *Nat. Nanotechnol.* **2015**, *10*, 865−869.
(35) Zharnikov, M.; Grunze, M. *J. Phys.: Condens. Matter* **2001**, *13*, 11333−11365.
(36) Wang, C.-F.; O'Callahan, B. T.; Kurouski, D.; Krayev, A.; Schultz, Z. D.; El-Khoury, P. Z. *J. Phys. Chem. Lett.* **2020**, *11*, 5890−5895.
(37) Wang, R.; Li, J.; Rigor, J.; Large, N.; El-Khoury, P. Z.; Rogachev, A. Y.; Kurouski, D. *J. Phys. Chem. C* **2020**, *124*, 2238−2244.
(38) Bhattarai, A.; Cheng, Z.; Joly, A. G.; Novikova, I. V.; Evans, J. E.; Schultz, Z. D.; Jones, M. R.; El-Khoury, P. Z. *J. Phys. Chem. Lett.* **2020**, *11*, 1795−1801.
(39) Zhu, W.; Esteban, R.; Borisov, A. G.; Baumberg, J. J.; Nordlander, P.; Lezec, H. J.; Aizpurua, J.; Crozier, K. B. *Nat. Commun.* **2016**, *7*, No. 11495.
(40) Zhu, W.; Crozier, K. B. *Nat. Commun.* **2014**, *5*, No. 5228.
(41) Kravtsov, V.; Berweger, S.; Atkin, J. M.; Raschke, M. B. *Nano Lett.* **2014**, *14*, 5270−5275.
(42) Hajisalem, G.; Nezami, M. S.; Gordon, R. *Nano Lett.* **2014**, *14*, 6651−6654.

https://doi.org/10.1021/acs.analchem.1c03004
Anal. Chem. 2021, 93, 15358−15364